Impact Analysis for the Planning of Targeted Non-Slippage Impacts of Robot Manipulators

Annika Kirner and Christian Ott, *Fellow, IEEE*

***Abstract*—Some impact tasks for robot manipulators, like stamping, demand that the end-effector does not slip off the target at the contact transition. We refer to this class of impacts as *targeted non-slippage impacts* and provide solutions to perform them. We present a model-based analysis and provide impact configurations and corresponding sets of joint space approach directions, under which the targeted non-slippage impact can be obtained. We show that the task space approach direction corresponding to a target configuration is unique and refer to it as the *non-slippage impact direction* (NSID). By means of an exemplary system, we demonstrate the target dependence of the NSID. The analysis presented in this work can be utilized for the planning of targeted non-slippage impact applications. We address two aspects in more detail. First, we discuss an NSID based choice of the impact target. Moreover, we introduce non-slippage impact paths (NSIPs) as possible approach paths of a target, which directly deduce from the proposed theory. The theoretic results are validated in experiments with a torque controlled robot.**

***Index Terms*—Dynamics, contact modeling, impact-aware planning and control.**

I. Introduction

TRADITIONALLY, robot manipulation tasks involving contact transitions have mostly been performed at vanishing contact velocities. There are two main reasons. First, the impact introduces a fast change in the system velocities which yields challenges for the control [1]. Second, conventional robotic hardware may be damaged by the large impulsive forces acting at the impact [2]. However, incorporating intentional impacts at non-zero velocities can significantly improve the performance of manipulation tasks. Moreover, some applications, like hammering or stamping, explicitly require the occurrence of an impact. With elastic robots, furthermore, robust hardware is now available to perform such tasks [3]. Consequently, the field of impact-aware robotics has recently gained increasing attention.

Manuscript received 9 August 2023; accepted 27 December 2023. Date of publication 29 January 2024; date of current version 9 February 2024. This letter was recommended for publication by Associate Editor Y. Sun and Editor H. Liu upon evaluation of the reviewers' comments. This work was supported in part by the European Research Council (ERC) through the European Union's Horizon 2020 Research and Innovation Programme under Grant 819358. *(Corresponding author: Annika Kirner.)*

Annika Kirner is with the Automation and Control Institute, TU Wien, 1040 Vienna, Austria (e-mail: kirner@acin.tuwien.ac.at).

Christian Ott is with the Automation and Control Institute, TU Wien, 1040 Vienna, Austria, and also with the Institute of Robotics and Mechatronics, German Aerospace Center (DLR), 82234 Wessling, Germany (e-mail: christian.ott@tuwien.ac.at).

This letter has supplementary downloadable material available at https://doi.org/10.1109/LRA.2024.3359536, provided by the authors.

Digital Object Identifier 10.1109/LRA.2024.3359536

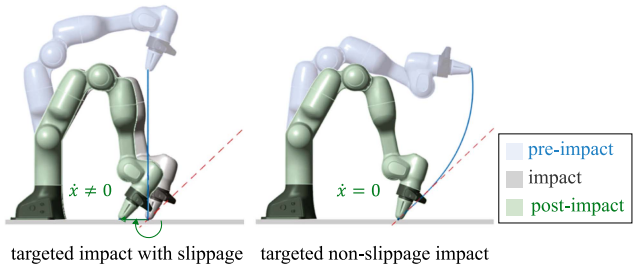

Fig. 1. Classification of robotic impact scenarios based on the post-impact task velocities. In the left case, the end-effector slips off the task space target defined by its Cartesian coordinate $\mathbf{x}$ after the impact. In the right case, the task coordinate is kept constant (targeted non-slippage impact).

Works include modeling of the impact event, e.g. [4], [5], [6], [7], detecting them [8], planning, e.g. [9], [10] or impact-aware control, e.g. [11], [12].

By means of the tangential relative velocity of two colliding bodies during and after the impact, two modes can be distinguished. Depending on the pre-impact state of the bodies, their inertial and elastic properties, and the friction coefficient, they will either remain at zero relative tangential velocity, i.e. stick, or they will slide, as has been analyzed in detail for rigid bodies e.g. in [13] in two dimensions and in [14] and [15] for the three dimensional case. Also, in impact experiments with robot manipulators, sliding behavior of the end-effector was observed after the impact [4], [7].

Several impact tasks require the end-effector to remain at the target after the impact. If sliding is avoided, damage of the work piece can be prevented (e.g. a stamping tool should not slide along the surface after the stamping) and a force can be exerted on the target as soon as contact is established. Thus, in this work, we address, what we refer to as *targeted non-slippage impacts*. A contact transition shall be performed with the end-effector of a robot manipulator at a pre-defined task space target and at non-vanishing pre-impact velocity, such that the end-effector keeps the task coordinate after the impact (cf. Fig. 1).

We suggest to not handle the slippage by a feedback controller only, as impact effects are ideally instantaneous by definition. Instead, we propose to use an impact model to plan the approach direction to an appropriately chosen target, such that post-impact velocities can be avoided. For this work, we assume fully inelastic and frictionless impacts. We thus aim at obtaining the non-slippage behavior solely based on inertial and kinematic properties without relying on contact or joint friction. However, the results are applicable for frictional contacts as well.

The main contribution of this letter is a model-based solution of the targeted non-slippage impact problem. We

- derive the *non-slippage impact direction* (NSID) associated with a given target configuration, under which it can be impacted without slippage, and
- analyze the target dependence of the NSID for an exemplary system.

Further, we address two possible applications of the theoretical results to the planning of impact tasks:

- a choice of targets based on the NSID, and
- approach paths, which are directly deduced from the theory.

Our work is complementary to [11]. There, the impact invariant subspace was introduced to be the space of approach velocities which remain unaffected by the impact. The space was utilized to formulate a controller, which is less sensitive towards uncertainties, such as the timing of the impact [11]. In our work, the impact shall be exploited to stop task velocities. Thus, we systematically choose approach velocities, which are affected by the impact, in the following.

This letter is structured as follows. The targeted non-slippage impact is defined in Section II. Non-slippage impact approach directions for a given target are derived in Section III. Section IV analyses the target dependence of the approach directions in task space for a planar example. Section V discusses consequences of the presented results for the planning. The theoretic results are validated experimentally in Sections VI and VII concludes this work.

II. Fundamentals and Preliminaries

A. Constrained Robot Dynamics and Impact Model

Consider the robot dynamics in the form

$$\mathbf{M}(\mathbf{q})\ddot{\mathbf{q}} + \mathbf{h}(\mathbf{q}, \dot{\mathbf{q}}) = \boldsymbol{\tau} + \boldsymbol{\tau}_{\text{contact}}. \tag{1}$$

Therein, the vectors of the n joint positions, velocities and accelerations are denoted by $\mathbf{q}, \dot{\mathbf{q}}, \ddot{\mathbf{q}} \in \mathbf{R}^n$, respectively. The positive definite, symmetric inertia matrix is denoted by $\mathbf{M}(\mathbf{q}) \in \mathbf{R}^{n\times n}$. The Coriolis- and centrifugal terms and the gravity torques are contained in $\mathbf{h}(\mathbf{q}, \dot{\mathbf{q}}) \in \mathbf{R}^n$. The joint torques are denoted by $\boldsymbol{\tau} \in \mathbf{R}^n$. The external torques $\boldsymbol{\tau}_{\text{contact}}$ result from contact forces with the environment.

The Cartesian task coordinate $\mathbf{x} \in \mathbf{R}^m$, with $m \leq n$, is given by the forward kinematics function $\mathbf{x} = \mathbf{f}(\mathbf{q})$. The task velocity $\dot{\mathbf{x}} = \frac{\partial \mathbf{f}(\mathbf{q})}{\partial \mathbf{q}}\dot{\mathbf{q}} = \mathbf{J}(\mathbf{q})\dot{\mathbf{q}}$ is computed via the task Jacobian $\mathbf{J}(\mathbf{q}) \in \mathbf{R}^{m\times n}$. In this work, the end-effector is assumed to be subject to one holonomic inequality constraint $\varphi(\mathbf{x}) \geq 0$, where $\varphi = 0$ specifies the contact surface. Thus,

$$\phi(\mathbf{q}) := (\varphi \circ \mathbf{f})(\mathbf{q}) \geq 0, \tag{2}$$

can be introduced as the joint space constraint, where $\circ$ refers to the function composition operator. The constraint Jacobian $\mathbf{A}(\mathbf{q}) \in \mathbf{R}^{1\times n}$ is given by $\mathbf{A}(\mathbf{q}) = \frac{\partial \phi(\mathbf{q})}{\partial \mathbf{q}}$.

The transition from free motion (i.e. $\phi(\mathbf{q}) > 0$ and thus $\boldsymbol{\tau}_{\text{contact}} = \mathbf{0}$) to a constrained phase (i.e. $\phi(\mathbf{q}) = 0 = \text{const.}$ and $\boldsymbol{\tau}_{\text{contact}} = \mathbf{A}(\mathbf{q})^T\lambda \neq \mathbf{0}$, where $\lambda > 0$ is the contact force) is considered to be an impact. It is assumed that the joint velocities jump from the finite pre-impact value $\dot{\mathbf{q}}^-$ to a finite post-impact value $\dot{\mathbf{q}}^+$, while $\mathbf{q}$ is not affected by the impact [2]. By integration of the dynamics (1) over the infinitesimal duration $\Delta t \to 0$ of the impact, one obtains the impact equation [2], [16]

$$\mathbf{M}(\mathbf{q})(\dot{\mathbf{q}}^+ - \dot{\mathbf{q}}^-) = \mathbf{A}^T(\mathbf{q})\Lambda, \tag{3}$$

where $\Lambda \in \mathbf{R}$ is an impulsive force.

In this work, the impact is assumed to be fully inelastic, which implies that all velocities normal to the constraint in Euclidean space vanish after the impact, i.e. $\mathbf{A}(\mathbf{q})\dot{\mathbf{q}}^+ = 0$. Furthermore, we assume a frictionless impact. The post-impact joint velocity can then be derived (cf., e.g. [4]) from (3) as

$$\dot{\mathbf{q}}^+ = \underbrace{(\mathbf{I} - \mathbf{M}^{-1}\mathbf{A}^T(\mathbf{A}\mathbf{M}^{-1}\mathbf{A}^T)^{-1}\mathbf{A})}_{:=\mathbf{P}(\mathbf{q})}\dot{\mathbf{q}}^-, \tag{4}$$

where $\mathbf{P}(\mathbf{q})$ can be identified to be a dynamically consistent projector, which maps the pre-impact joint velocity $\dot{\mathbf{q}}^-$ to the null space of the constraint Jacobian $\mathbf{A}(\mathbf{q})$.

Despite its idealized inelastic impulse, this model has been commonly applied in robotics [11], [12]. Recently, several works have addressed experimental evaluations and adjustments of the model to account for elasticity introduced by serial elastic actuators with high joint stiffness [4], [5], [6], [7]. Predictions of the model have been reported to be less precise than predictions considering the robot as one composite rigid body for kinematically controlled robots [6], [7]. However, the model (4) can satisfactorily predict the post-impact response of torque controlled robots [4], especially if a contribution of the apparent motor inertia is added upon the inertia matrix $\mathbf{M}(\mathbf{q})$ [5]. Given the results [4], [5], we expect that a solution to the targeted non-slippage impact problem based on the model (4) can be applied to common torque controlled robots.

B. Targeted Non-Slippage Impacts

Let $\mathbf{x}_*$ be a target on the constraint surface, i.e. it holds $\varphi(\mathbf{x}_*) = 0$. We define a targeted non-slippage impact to be an impact performed at $\mathbf{x}_*$ at a non-vanishing pre-impact contact velocity $\dot{\phi}(\mathbf{q}_*, \dot{\mathbf{q}}^-)$, such that any post-impact task velocities $\dot{\mathbf{x}}^+$ vanish. For this work, we utilize the dynamics and impact model defined in Section II-A. Thus, we focus on the worst-case scenario of a perfectly frictionless contact and aim at preventing slippage through the kinematic and inertial properties of the robot. The configuration $\mathbf{q}_*$ at the impact and the non-zero pre-impact joint velocity $\dot{\mathbf{q}}^-$ then need to satisfy

$$\dot{\mathbf{x}}^+ = \mathbf{J}(\mathbf{q}_*)\dot{\mathbf{q}}^+ = \mathbf{J}(\mathbf{q}_*)\mathbf{P}(\mathbf{q}_*)\dot{\mathbf{q}}^- = \mathbf{0}, \tag{5a}$$

$$\mathbf{x}_* = \mathbf{f}(\mathbf{q}_*), \tag{5b}$$

$$\dot{\phi}(\mathbf{q}_*, \dot{\mathbf{q}}^-) = \mathbf{A}(\mathbf{q}_*)\dot{\mathbf{q}}^- < 0. \tag{5c}$$

Here, (5c) ensures that the target is approached from the admissible side. In the following, we use the term "slippage" for both translational and rotational post-impact movements of the end-effector with respect to the target.

III. Non-Slippage Impact Approach Velocities

In this section, (5) is solved for a given, fixed target configuration $\mathbf{q}_*$ satisfying (5b).

A. Preventing Post-Impact Joint Velocities: The Stop-on-Impact Direction

First, the special case of vanishing joint velocities is treated. It is straightforward that a pre-impact joint velocity $\dot{\mathbf{q}}^- = \dot{\mathbf{q}}_* \neq \mathbf{0}$ that fulfills $\dot{\mathbf{q}}^+ = \mathbf{P}(\mathbf{q}_*)\dot{\mathbf{q}}_* = \mathbf{0}$, also fulfills (5a). Every solution $\dot{\mathbf{q}}_*$ of this sub-problem can be expressed as

$$\dot{\mathbf{q}}_* = \nu \mathbf{M}^{-1}(\mathbf{q}_*)\mathbf{A}^T(\mathbf{q}_*), \tag{6}$$

with a scaling factor $\nu < 0$.[1] The velocity $\dot{\mathbf{q}}_*$ will be referred to as the *stop-on-impact (approach) direction* in the following, where the term *direction* is due to the fact that $\dot{\mathbf{q}}_*$ can be scaled arbitrarily with $\nu < 0$. The stop-on-impact direction is co-linear to the one-dimensional[2] null space of $\mathbf{P}(\mathbf{q}_*)$. It describes the unique direction along which velocity jumps occur [11] and is considered to be the normal direction of the constraint with respect to the kinetic metric [16].

It is notable that the desired value of the impulsive force Λ can be directly set by the choice of the scale ν. As $\dot{\mathbf{q}}^+ = \mathbf{0}$ holds, plugging $\dot{\mathbf{q}}^- = \dot{\mathbf{q}}_*$ in (3) yields $\nu = -\Lambda$. With the condition $\nu < 0$, (6) thus defines an approach velocity that yields a positive impulsive force upon the impact. Hence, the constraint is approached from the admissible side, which can also be verified from plugging (6) in (5c): the inequality $\dot{\phi}^- = \nu \mathbf{A}(\mathbf{q}_*)\mathbf{M}^{-1}(\mathbf{q}_*)\mathbf{A}^T(\mathbf{q}_*) < 0$ is fulfilled for $\nu < 0$.

B. Preventing Post-Impact Task Velocities

The stop-on-impact approach direction $\dot{\mathbf{q}}_*$ complements a given, fixed $\mathbf{q}_*$ to one particular solution of (5). For a redundant robot manipulator with $n > m$, further approach directions for the same $\mathbf{q}_*$ exist.

Theorem 1: Given a configuration $\mathbf{q}_*$ which fulfills (5b), any corresponding pre-impact joint space velocity $\dot{\mathbf{q}}^- = \dot{\mathbf{q}}_x$ of the form

$$\dot{\mathbf{q}}_x := \dot{\mathbf{q}}_* + \dot{\mathbf{q}}_n, \tag{7}$$

yields a non-slippage impact at $\mathbf{x}_*$, i.e. it fulfills (5). Therein, $\dot{\mathbf{q}}_n \in \mathbf{R}^n$ is an arbitrary vector in the $(n-m)$-dimensional null space of the task Jacobian: $\dot{\mathbf{q}}_n \in \ker(\mathbf{J}(\mathbf{q}_*))$.

Proof: As the constraint has been imposed on the end-effector coordinate, it holds: $\text{range}(\mathbf{A}(\mathbf{q})) \subseteq \text{range}(\mathbf{J}(\mathbf{q}))$. Thus, every $\dot{\mathbf{q}}_n \in \ker(\mathbf{J}(\mathbf{q}))$ is also in the range of the projector given by $\text{range}(\mathbf{P}(\mathbf{q})) = (\text{range}(\mathbf{A}^T(\mathbf{q})))^\perp$. Consequently,

$$\dot{\mathbf{x}}^+ = \mathbf{J}(\mathbf{q}_*)\dot{\mathbf{q}}^+ = \mathbf{J}(\mathbf{q}_*)\mathbf{P}(\mathbf{q}_*)\dot{\mathbf{q}}_x = \mathbf{J}(\mathbf{q}_*)\dot{\mathbf{q}}_n = \mathbf{0} \tag{8}$$

holds and (5a) is fulfilled. For (5c) it can be shown that $\dot{\phi}^- = \nu \mathbf{A}(\mathbf{q}_*)\mathbf{M}^{-1}(\mathbf{q}_*)\mathbf{A}^T(\mathbf{q}_*) < 0$ holds, which concludes the proof. □

From (8) it becomes evident that the non-slippage behavior is obtained despite a remaining joint velocity $\dot{\mathbf{q}}^+ = \mathbf{q}_n$. This results from the null space velocity $\dot{\mathbf{q}}_n$ added to $\dot{\mathbf{q}}_*$ in (7), which is retained over the impact. It can be shown that any joint space approach velocity $\dot{\mathbf{q}}^-$ fulfilling (5) can be obtained from (7).

In order to plan the impact, the task space approach direction corresponding to $\dot{\mathbf{q}}_x$ is of special interest. It can be shown to be

$$\dot{\mathbf{x}}_* = \mathbf{J}(\mathbf{q}_*)\dot{\mathbf{q}}_x = \mathbf{J}(\mathbf{q}_*)\dot{\mathbf{q}}_* = \nu \mathbf{J}(\mathbf{q}_*)\mathbf{M}^{-1}(\mathbf{q}_*)\mathbf{A}^T(\mathbf{q}_*), \tag{9}$$

where we define $\dot{\mathbf{x}}_*$ as the *non-slippage impact direction* (NSID) associated with $\mathbf{q}_*$. It is thus the unique task space approach direction yielding a non-slippage impact for a given $\mathbf{q}_*$ and cannot be modified by a null space movement $\dot{\mathbf{q}}_n$. It is notable that the NSID depends on $\mathbf{q}_*$. Thus, in general, it is possible to modify it by reconfigurations in the null space, or by shifting the task space target.

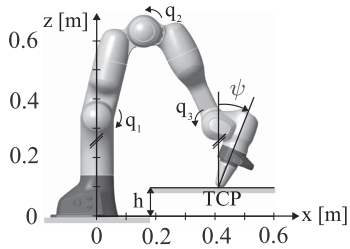

Fig. 2. Planar system with three serial joints based on the "Franka Research 3" robot placed in front of a horizontal table of height h.

C. Extension to Frictional Impacts

The presented approach directions yielding a non-slippage impact at the target $\mathbf{q}_*$ have been derived for a frictionless contact. The corresponding impulsive contact force is perpendicular to the contact surface. Intuitively, it can be understood that contact friction is beneficial for the non-slippage task. Thus, it seems plausible that the results of this work can be applied directly to perform targeted non-slippage impacts of frictional surfaces.

IV. Task Space Impact Analysis

In this section, we focus on the NSID from (9) and analyze how it can be modified by reconfiguring the robot in the feasible configuration space for an exemplary system.

A. Planar System With Three Degrees of Freedom

To keep the results of the analysis condensed, the planar, non-redundant system, depicted in Fig. 2 is addressed as an example.[3] It corresponds to the "Franka Research 3" robot, however, only the second, fourth and sixth joints are included in this planar case study. Their joint positions are stacked in the vector $\mathbf{q} \in \mathbf{R}^3$. The remaining joints of the original robot are assumed to be rigid and in their zero configuration. The official kinematic parameters of the robot are taken from [17]. An impact tool is mounted

[1] Note that $\mathbf{P}(\mathbf{q}_*)\dot{\mathbf{q}}_* = \mathbf{0}$ holds by definition of $\mathbf{P}(\mathbf{q}_*)$ in (4).

[2] Remember that only one inequality constraint is considered.

[3] The analysis can be performed with systems featuring more degrees of freedom or a three-dimensional task space accordingly. In case of redundancy, the null space parameters need to be varied, besides the task space target, to analyze their effects on the NSID.

at the end-effector flange, yielding an offset of the tool center point (TCP) of 0.0825 m (cf. Fig. 2). The mass of the tool is assumed to be negligible. For the dynamic parameters of the robot, the estimates determined in [18] are utilized. However, the apparent reflected motor inertia is added to the inertia matrix $\tilde{\mathbf{M}}(\mathbf{q})$ obtaining the total inertia matrix $\mathbf{M}(\mathbf{q}) = \tilde{\mathbf{M}}(\mathbf{q}) + \mathbf{B}$ with $\mathbf{B} = \mathrm{diag}([0.6 \quad 0.45 \quad 0.2])$ [5].[4]

The task coordinate $\mathbf{x} = [x \quad z \quad \psi]^T \in \mathbf{R}^3$ contains both the position and the orientation ψ of the end-effector, as defined in Fig. 2. A table of height $h \in \mathbf{R}$ with a surface normal in z-direction acts as an inequality constraint on the end-effector and enforces that it remains above the surface of the table. It holds $\phi(\mathbf{q}) = z - h = [0 \quad 1 \quad 0]\mathbf{f}(\mathbf{q}) - h$.

In the following, it is assumed that the robot is always in an "elbow up" configuration. Thus, given $\mathbf{x}_*$, the solution $\mathbf{q}_*$ of (5b) is unique out of kinematic singularities. Consequently, we can focus on $\mathbf{x}_*$ and analyze the effects on the NSID in place of $\mathbf{q}_*$ in the following. Approaches under the NSID always yield $\dot{\mathbf{q}}^+ = \mathbf{0}$ for this non-redundant example.

B. Effects of Varying the Task Space Target on the NSID

In the following, every component of the target $\mathbf{x}_* = [x_* \quad z_* \quad \psi_*]^T$, where $z_* = h$ holds, is varied and the effects on the NSID are analyzed. For comparison, the NSIDs are evaluated at a constant pre-impact kinetic energy of $T^- = \frac{1}{2}\dot{\mathbf{q}}_*^T \mathbf{M}(\mathbf{q}_*)\dot{\mathbf{q}}_* = 0.2\,\mathrm{J}$, which provides the target-dependent scale $\nu = (2\,T^-(\mathbf{A}(\mathbf{q}_*)\mathbf{M}(\mathbf{q}_*)^{-1}\mathbf{A}(\mathbf{q}_*)^T)^{-1})^{\frac{1}{2}}$.

The NSID of the considered system can be split into the rotational part $\dot{\psi}_*$ and the translational part $[\dot{x}_* \quad \dot{z}_*]^T$.

1) Rotational Component of the NSID: The distribution of the rotational component of the NSID over the relevant task space is depicted in Fig. 3.[5]

Fig. 3(a) shows the variation of $\dot{\psi}_*$ with ψ_* at various values for x_* and at constant $z_* = 0.0$ m, whereas $x_* = 0.4$ m is kept constant for the results in Fig. 3(b). There z_* is varied. Note that $\dot{\psi}_*$ is considerably affected by ψ_* for every target position. Adjusting the target position at a constant value of ψ_* shows comparably smaller effects.

2) Translational Component of the NSID: Fig. 4 depicts the *translational approach angle* α_* defined by $\tan(\alpha_*) = -\frac{\dot{x}_*}{\dot{z}_*}$ which describes the translational part of the NSID. Again, the effects of ψ_* on α_* are considered at various x_* in Fig. 4(a), while z_* is varied in Fig. 4(b). Graphical representations of the translational approach directions for varying x_*, z_*, and ψ_* are provided in Fig. 4(c)–(e), respectively. We notice that α_* is clearly affected by ψ_* for every considered target position. As compared to the rotational component, the effects of varying the position at a constant ψ_* are stronger.

3) Summary: We summarize the following properties for the given system: The NSID can be modified by every component of the target $\mathbf{x}_*$. However, effects of the target position predominantly appear towards the boundaries of the considered task space and for the translational part of the NSID. In contrast, the NSID clearly varies with the target orientation ψ_* for every considered target position.

Of course, the effects of each component of the target $\mathbf{x}_*$ or $\mathbf{q}_*$ on the NSID strongly depend on the considered robotic system and the definition of the task coordinate. The analysis, exemplified for the three pitch axes of the Franka Emika robot in this section, can identify relevant components, which can be useful for the planning of impact tasks.

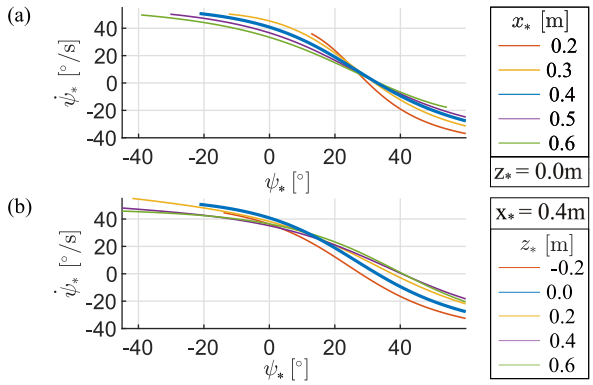

Fig. 3. Rotational component $\dot{\psi}_*$ of the NSID for varying $\mathbf{x}_* = [x_* \quad z_* \quad \psi_*]^T$: (a) variation over ψ_* and x_* and (b) variation over ψ_* and z_*.

V. Consequences for the Planning of Targeted Non-Slippage Impact Tasks

The analysis presented in the previous sections allows a multitude of applications and provides a basis to plan specific targeted non-slippage impact tasks for robot manipulators. In this section, we focus on two important aspects: an NSID based choice of the target in Section V-A and a class of possible approach paths in Section V-B. A more comprehensive application of the presented theory to targeted non-slippage impact problems is subject to future work.

A. NSID Dependent Choice of the Target

In this section, again the planar system from Section IV is considered. We address an NSID based choice of a target location $\mathbf{x}_*$, i.e. we discuss solutions of (9) for $\mathbf{x}_* = f(\mathbf{q}_*)$, where the desired NSID is, at least partially, given by the task.[6] In order to remain in a reasonable part of the task space, the bounds $0.3\,\mathrm{m} \leq x_* \leq 0.5\,\mathrm{m}$ and $-0.2\,\mathrm{m} \leq z_* \leq 0.4\,\mathrm{m}$ for the target position are defined and it is assumed that small $|\psi_*|$ are desired. Two common cases are discussed: a vertical approach to the surface of the table and an approach at constant end-effector orientation.

1) Vertical Approach: Assume a hammering task shall be performed. The nail can be placed arbitrarily on the surface of the table of adjustable height. To not bend the nail, it shall

[4]The additional contribution $\mathbf{B}$ also improves the conditioning of $\mathbf{M}(\mathbf{q}_*)$, which is beneficial for the inversion required for (6).

[5]Only feasible configurations which do not violate joint space boundaries are included in every following plot.

[6]Note that it has been assumed that $\mathbf{x}_*$ uniquely maps to $\mathbf{q}_*$ for the planar system. Thus, we express the NSID $\dot{\mathbf{x}}_*(\mathbf{x}_*)$ as well as its components $\alpha_*(\mathbf{x}_*)$ and $\dot{\psi}_*(\mathbf{x}_*)$ directly as functions of $\mathbf{x}_*$ in the following.

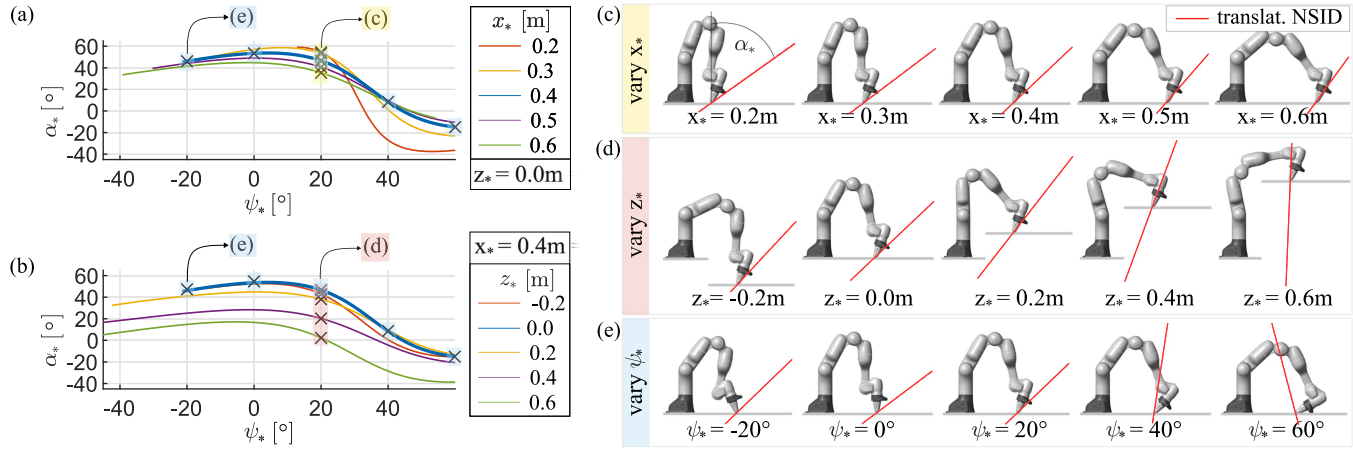

Fig. 4. Translational component of the NSID expressed via the translational approach angle α_* for varying components of $\mathbf{x}_* = [x_* \quad z_* \quad \psi_*]^T$.

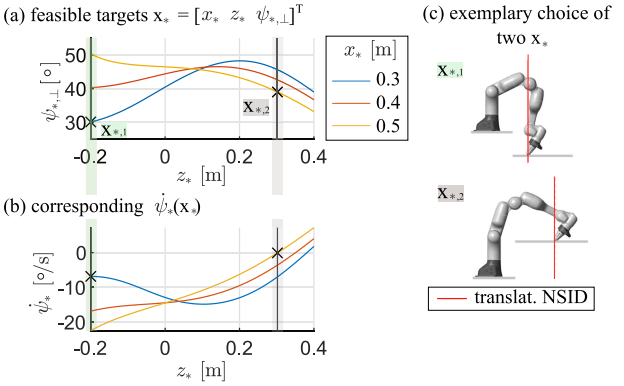

Fig. 5. Targets $\mathbf{x}_*$ yielding an NSID such that the table surface can be approached vertically (a). The exemplary choice $\mathbf{x}_{*,1}$ in (c) minimizes $\psi_{*,\perp}$, whereas $\mathbf{x}_{*,2}$ minimizes $|\dot{\psi}_*|$ from (b).

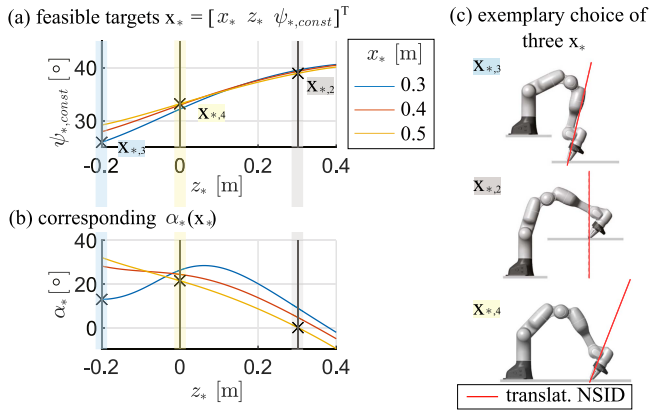

Fig. 6. Targets corresponding to a NSID with $\dot{\psi}_* = 0.0\,^\circ/\mathrm{s}$ for the planar system (a). The three specific choices in (c) are chosen such that they minimize $\psi_{*,\mathrm{const}}$, minimize the corresponding $|\alpha_*|$ as depicted in (b) (cf. Fig. 5), and qualitatively trade-off between both quantities, from top to bottom, respectively.

be impacted *vertically*, i.e. in z-direction. Moreover, the end-effector shall not slip off the nail after the impact. To achieve these goals, a target $\mathbf{x}_*$ needs to be chosen yielding an NSID with $\alpha_*(\mathbf{x}_*) = 0.0\,^\circ$. The rotational component $\dot{\psi}_*(\mathbf{x}_*)$ is not predefined. Still, we assume that a small absolute value of $\dot{\psi}_*(\mathbf{x}_*)$ is preferred, if feasible.

From the results of Section IV, it can already be concluded that targets exist that correspond to suitable NSIDs (cf. the roots of $\alpha_*(\mathbf{x}_*)$ in Fig. 3). In order to choose suitable ones, first, all possible targets $\mathbf{x}_*$ yielding an NSID with $\alpha_*(\mathbf{x}_*) = 0.0\,^\circ$ are determined. Therefore, the position $[x_* \quad z_*]^T$ is varied in the feasible range and the corresponding roots $\psi_{*,\perp}$ of $\alpha_*(\mathbf{x}_* = [x_* \quad z_* \quad \psi_{*,\perp}]^T)$ are approximated numerically. Every resulting $\mathbf{x}_*$ as depicted in Fig. 5(a) yields the desired vanishing translational approach angle. The corresponding $\dot{\psi}_*(\mathbf{x}_*)$ are plotted in Fig. 5(b).

We choose two targets $\mathbf{x}_*$ based on the criteria for ψ_* and $\dot{\psi}_*(\mathbf{x}_*)$. They are visualized in Fig. 5(c). The first target $\mathbf{x}_{*,1} \approx [0.3\ \mathrm{m} \quad -0.2\ \mathrm{m} \quad 30.1\,^\circ]^T$ minimizes $\psi_{*,\perp}$ in the considered task space. The second one $\mathbf{x}_{*,2} \approx [0.5\ \mathrm{m} \quad 0.30\ \mathrm{m} \quad 38.9\,^\circ]^T$ features a larger target orientation, however, this orientation can be kept constant for the approach as $\dot{\psi}_*(\mathbf{x}_{*,2}) = 0.0\,^\circ/\mathrm{s}$ holds.

2) Approach at Constant End-Effector Orientation: Applications, such as stamping or tapping two components together with the bottom surface of a flat impact tool, require a targeted non-slippage impact under a given, constant end-effector orientation. Fig. 6(a) shows the $\psi_{*,\mathrm{const}}$ for the planar system that complement the vector $\mathbf{x}_* = [x_* \quad z_* \quad \psi_{*,\mathrm{const}}]^T$ for varying x_* and z_*, such that the corresponding $\dot{\psi}_*(\mathbf{x}_*)$ vanishes. An impact under the orientation imposed by the tool can only be performed, if it is contained in the range of $26.0^\circ \leq \psi_{*,\mathrm{const}} \leq 40.4^\circ$.

We exemplarily depict three configurations, for which no specific value of ψ_* is assumed to be given.[7] Target $\mathbf{x}_{*,3} \approx [0.3\ \mathrm{m} \quad -0.2\ \mathrm{m} \quad 26.0\,^\circ]^T$ minimizes $\psi_{*,\mathrm{const}}$ in the considered task space. The angles $\alpha_*(\mathbf{x}_*)$ belonging to every $\mathbf{x}_*$ are provided in Fig. 6(b). Target $\mathbf{x}_{*,2}$ has already been mentioned for the previous application, as it yields an approach at constant end-effector orientation that is vertical. It thus minimizes $|\alpha_*(\mathbf{x}_*)|$. Finally, $\mathbf{x}_{*,4} \approx [0.5\ \mathrm{m} \quad 0.0\ \mathrm{m} \quad 33.2\,^\circ]^T$ was

[7]In practice this would require that the tool can be mounted in various orientations.

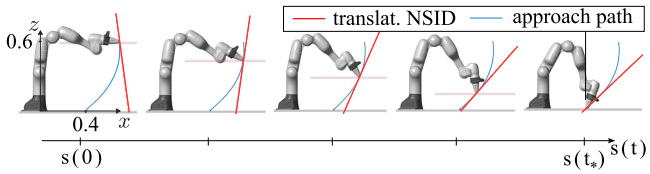

Fig. 7. Sequential illustration of the stop-on-impact path corresponding to the target $\mathbf{x}_* = [0.4\ \mathrm{m} \quad 0.0\ \mathrm{m} \quad 20.0°]^T$, which is reached in the last frame.

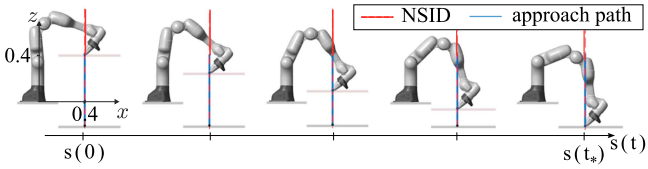

Fig. 8. Sequential illustration of the vertical NSIP of a target $x_* = 0.4$ m, on a table of unknown height.

chosen manually such that it qualitatively trades off between the approach angle and the end-effector orientation.

3) Conclusion: Starting from the results of Section IV, showing that the desired NSIDs with $\alpha_* = 0.0°$ and $\dot{\psi}_* = 0.0\,°/\mathrm{s}$ are feasible for the planar system, we performed a more detailed analysis here, to qualitatively select and discuss optimal targets. Such an analysis can be an important element of a future planning framework.

B. Non-Slippage Impact Approach Paths

Given a target and an approach direction in joint or task space, suitable approach paths can be planned. In the following, we discuss one class of paths, which directly deduces from the proposed theory.

1) Definition of Non-Slippage Impact Paths: Consider (7) as a differential equation in $\mathbf{q}(s)$, i.e.

$$\frac{\partial \mathbf{q}(s)}{\partial s} = \dot{\mathbf{q}}_*(\mathbf{q}(s)) + \dot{\mathbf{q}}_n(\mathbf{q}(s)), \tag{10}$$

where s is a time parametrization. Numerical integration backwards in time with initial condition $\mathbf{q}_*$ yields a *non-slippage impact path* (NSIP) approaching $\mathbf{q}_*$. Thus, a NSIP of a target $\mathbf{q}_*$ is defined by two properties. First, the constraint function $\phi(\mathbf{q}_*(s))$ monotonically decreases to $\phi(\mathbf{q}_*) = 0$ along the path (cf. (5c)). Second, $\mathbf{x}(s) = \mathbf{f}(\mathbf{q}(s))$ is tangential to the instantaneous NSID for every s.

For a non-redundant system, the NSIP approaching a given target $\mathbf{q}_*$ is unique and can be considered a *stop-on-impact path*. However, it cannot be adjusted to meet requirements, including joint limits, which might restrict its practical relevance. Introducing null-space contributions $\dot{\mathbf{q}}_n(\mathbf{q}(s))$ for a redundant system modifies the NSIP in joint space. However, the re-configuration of the robot along the path also affects the NSID and, thus, the tangent of the task-space path. Hence, the null-space motions can shape the NSIP in joint and task spaces. This shall be exemplified in the following.

2) Examples: Consider again the planar system. Assume a non-slippage impact shall be performed at a target $x_* = 0.4$ m on the table surface with $h = 0.0$ m. We assume $\psi_* = 20.0°$ for the target orientation and compute the stop-on-impact path of the resulting target by backwards integration. A sequential illustration is provided in Fig. 7. Note that a non-slippage impact would be yielded along the path for a collision with a table of arbitrary height. However, $\mathbf{x}_*$ would not be reached in that case.

As a second example, $x_* = 0.4$ m shall be impacted without slippage in x-direction. The end-effector orientation ψ is thus considered to be a null space parameter for this application. The height h of the table is assumed to be unknown. In order to reach x_* despite the uncertainty, a vertical approach path $[x_* \quad z(s)]^T$ is chosen. A $\psi(s)$ shall be found, such that it holds $\alpha_*(s) = 0.0°$ for every s along the path. Consequently, null space movements shall align the NSID with the vertical approach path to turn the path into an NSIP.

We can directly utilize the results from Section V-A1. There, the $\psi_{*,\perp}$ complementing the positions $[0.4\ \mathrm{m} \quad z_*]^T$ to a three dimensional target $\mathbf{x}_*$ yielding $\alpha_*(\mathbf{x}_*) = 0.0°$ have been computed numerically for discrete values of z_* (cf. orange line in Fig. 5(a)). The path formed by the resulting $\mathbf{x}_*$ leading toward decreasing z-values represents the desired vertical NSIP. The sequential illustration in Fig. 8 demonstrates that the NSID remains vertical and thus aligned with the path.

3) Conclusion: NSIPs demonstrate core statements of this work: they represent the evolution of the NSID over the task space, which can be adjusted by re-configurations in the null space but not by instantaneous null space velocities. A more comprehensive and application-oriented treatment of approach paths and trajectories for targeted non-slippage impact tasks is beyond the scope of this letter and subject to future work.

VI. Experimental Validation

A. Experimental Setup

To demonstrate the practical relevance of the impact analysis, experiments are performed with a "Franka Research 3" robot [17] under torque control, which impacts a horizontal table. The surface with $h = 0.0$ m is melamine-coated, and the tip of the tool is made from PLA. To protect the robot, the tool contains a central part made of TPU. It is assumed that the diameter of the tool is negligible and that the impact always occurs between the tip of the tool and the table.

To approximate a planar system with three degrees of freedom, the joints 1, 3, 5, and 7 are regulated in their initial positions. Task space trajectories towards the targets are tracked utilizing the torque control interface of the robot. To visualize the uncontrolled slippage effects, the controller contributions for the x- and ψ-directions are switched to gravity compensation before the tip impacts the table based on the z-position of the end-effector.

We conduct experiments in two target configurations and two translational approach directions as depicted in Fig. 9. For both target configurations it holds $x_* = 0.4$ m. "Config. 0" features an upright end-effector, i.e. $\psi_* = 0.0°$. "Config. $\perp$" with $\psi_* = 44.4°$ has been chosen, such that it holds $\alpha_* = 0.0°$. Furthermore, we distinguish if the experiments have been performed

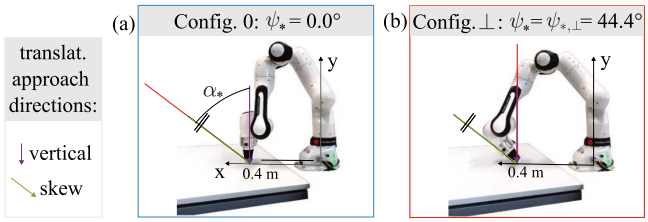

Fig. 9. Impact configurations and translational approach directions utilized in the experiments. For Config. 0, the translational component of the NSID aligns with the skew direction, whereas it is vertical for Config. $\perp$.

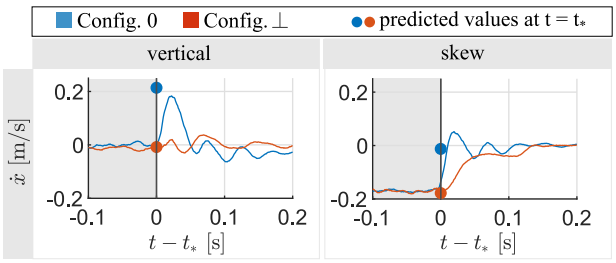

Fig. 10. Results of experiment #1. Post-impact velocities $\dot{x}$ can be reduced for a vertical impact of Config. $\perp$ and a skew impact of Config. 0.

under the "vertical" or "skew" translational approach direction. The vertical approach direction aligns with the translational NSID of Config. $\perp$, while the skew direction is defined by the translational approach angle $\alpha_* = 53.4°$ of Config. 0. Every desired approach velocity $\dot{\mathbf{x}}_d$ utilized in the following aligns with either of the two directions. It is chosen, such that it holds $\sqrt{\dot{x}_d^2 + \dot{z}_d^2} = 0.2\ \mathrm{m/s}$ for the desired translational velocity at the impact. The rotational component $\dot{\psi}_d$ is specified separately.

B. Experiment #1: Avoiding Translational Slippage

In the first set of experiments, we aim at avoiding translational slippage, while a post-impact angular velocity is assumed to be acceptable. Thus, ψ can be considered a null space parameter for this set. We perform the vertical and skew approach for each configuration. The pre-impact angular end-effector velocity is regulated at $\dot{\psi}_d = 0.0\,°/\mathrm{s}$. From the presented theory, we expect post-impact velocities in x-direction to be suppressed if the approach angle corresponds to α_*.[8] More precisely, a vertical impact of Config. 0 should provoke translational slippage, while it should be suppressed for Config. $\perp$. The opposite is expected for skew impacts.

The recorded velocities $\dot{x}$ are depicted in Fig. 10 in a short time window around the impact time t_*. The t_* has been determined manually as a post-processing step based on the drop in the total kinetic energy. Furthermore, the predicted value $\dot{x}^+$ at t_* calculated from the measured values $\mathbf{q}(t_*)$ and $\dot{\mathbf{q}}(t_*)$ via (4) and the kinematics is marked.

1) Vertical Approach: No component $\dot{x}$ exists before the impact for vertical approaches. Still, as expected, a slippage effect in this direction is provoked by the impact of Config. 0. We observe an increase of $\dot{x}$ up to almost the prediction $\dot{x}^+$ and an oscillatory decay afterwards. Conversely, $\dot{x}$ remains approximately constant and at the prediction $\dot{x}^+ \approx 0.0\ \mathrm{m/s}$ for Config. $\perp$. Note that the prediction $\dot{x}^+$ only approximately vanishes for the approaches under α_* due to tracking errors and uncertainties, e.g., introduced by the unmodeled diameter of the tooltip.

2) Skew Approach: The skew approaches feature a pre-impact velocity in x-direction. For Config. $\perp$ the end-effector slides along the surface of the table after the impact and the component $\dot{x}$ is only gradually reduced. A faster decay of $\dot{x}$ after the impact can be observed for Config. 0. Damped oscillations around $\dot{x} \approx 0.0\ \mathrm{m/s}$ occur, which approximately corresponds to the prediction $\dot{x}^+$ at the impact time.

3) Discussion: The results of this experiment demonstrate: i) that a target configuration (here Config. $\perp$) can be chosen to realize a desired approach direction (here a vertical approach) for a targeted non-slippage impact and ii) that post-impact velocities in x-direction can be significantly reduced, if the translational approach is under α_*.

Even though the predictions $\dot{x}^+$ calculated from the measurements at t_* almost vanish under approaches at α_*, the slippage cannot fully be suppressed. This might be caused by several modeling errors. First, the idealizing assumption of a fully inelastic impact is not fully valid. We observed a slight bouncing behavior of the end-effector tip during the experiments and the impact responses are oscillatory in general. This can be attributed to elasticity of the joints or the contact (cf. e.g. [4]). The predictions $\dot{x}^+$ correlate with the oscillatory responses, which is in line with the findings in [4], [5].[9] This matches the observation that slippage can still clearly be reduced using the proposed approach direction. Finally, model uncertainties, e.g. in the estimate of $\mathbf{B}$, might have resulted in an inaccurate planning of the NSID and the target.

C. Experiment #2: Including the Angular Velocity

In a second set of experiments, slippage in ψ shall be avoided on top of the translational slippage. Thus, for each configuration, we perform an approach under the full, three-dimensional NSID. As a baseline, we consider the approaches under α_* from experiment #1, i.e. the vertical approach for Config. $\perp$ and the skew approach for Config. 0. Thus, the baseline approach and the approach under the full NSID for each configuration only differ in $\dot{\psi}_d$. The value $\dot{\psi}_d = \dot{\psi}_*$ to fully align $\dot{\mathbf{x}}_d$ with the NSID is evaluated to be $\dot{\psi}_* \approx -20.5\,°/\mathrm{s}$ for Config. $\perp$ and $\dot{\psi}_* \approx 32.8\,°/\mathrm{s}$ for Config. 0.

1) Results: Fig. 11(a) and (b) show the recorded velocities $\dot{x}$ and $\dot{\psi}$, respectively. The slippage in x-direction for the approach under the full, three-dimensional NSID is small and closely corresponds to the baseline for each configuration. However, less slippage in $\dot{\psi}$ appears for the experiments under the full NSID. As expected, the predictions $\dot{\psi}^+$ approximately vanish. Also, the maximum peaks of the oscillatory responses are reduced.

[8] As ψ is treated as a null space parameter, the NSID is uniquely described by α_*.

[9] For quantitative comparisons between rigid body predictions and recorded oscillatory impact responses refer to [4], [5].

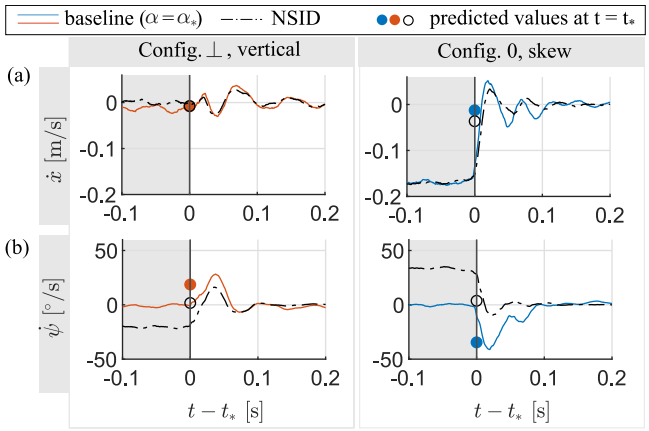

Fig. 11. Velocities $\dot{x}$ (a) and $\dot{\psi}$ (b) recorded for experiment #2. The baseline approaches correspond to the ones under α_* of experiment #1 depicted in Fig. 10.

2) Conclusion: The results verify that approaches under the NSID reduce slippage effects in all task space directions. Slippage in distinct task directions (here: the x-direction) can be selectively suppressed by reducing the non-slippage task coordinate. The value of the pre-impact velocities in the remaining (null space) directions (here: the ψ direction), does not affect the slippage in the relevant directions. Note that, for each configuration, $\dot{\psi}^- = \dot{\psi}_*$ of the approach under the full NSID approximately corresponds to the negative prediction $\dot{\psi}^+$ of the slippage induced by the baseline approach. This is consistent with the result that the deviation $\dot{\mathbf{q}}_n$ from $\dot{\mathbf{q}}_*$ in $\dot{\mathbf{q}}^- = \dot{\mathbf{q}}_x$ is retained over the impact. As ψ can be shown to uniquely parameterize the null space, this can be directly transferred to the angular end-effector velocities. For the null space contribution $\dot{\psi}_n$ corresponding to $\dot{\mathbf{q}}_n$ of the baseline approaches it holds: $\dot{\psi}^+ = \dot{\psi}_n = \dot{\psi}^- - \dot{\psi}_*$ (cf. (7)) which reduces to $\dot{\psi}^+ \approx -\dot{\psi}_*$ given $\dot{\psi}^- \approx \dot{\psi}_d = 0.0$ °/s.

VII. Conclusion

In this letter, targeted non-slippage impacts have been defined and solutions to perform them have been proposed. We provided the space of joint space approach directions resulting in a non-slippage impact at a given target $\mathbf{q}_*$. The NSID, i.e. the task space representation of these directions, is unique for a $\mathbf{q}_*$ and cannot be modified by null space velocities. However, we demonstrated a strong target dependence of the NSID for an exemplary system. Motivated by these results, we discussed an NSID based choice of impact targets for two applications. Moreover, we introduced NSIPs as possible approach paths, which directly deduce from the theoretical analysis.

Experiments validated that an approach under the proposed NSID can clearly reduce slippage effects despite assuming a fully inelastic and instantaneous impact. More comprehensive models could be utilized in the future to improve the prediction and to leverage stiction to yield non-slippage behavior systematically. There, data-driven approaches also seem promising.

Safety requirements of the robot restricted the pre-impact velocities in the experiments of this work. For elastic robots, larger approach velocities are feasible, which will potentially increase the slippage. Future works will thus examine targeted non-slippage impacts for elastic robots.

Acknowledgment

The authors would like to thank Alessandro Saccon for sharing his experience on impact experiments with Franka Emika robots and the results presented in [5] in advance. The authors acknowledge TU Wien Bibliothek for financial support through its Open Access Funding Programme.

References

[1] S. S. M. Salehian and A. Billard, "A dynamical-system-based approach for controlling robotic manipulators during noncontact/contact transitions," *IEEE Robot. Automat. Lett.*, vol. 3, no. 4, pp. 2738–2745, Oct. 2018.
[2] I. Walker, "Impact configurations and measures for kinematically redundant and multiple armed robot systems," *IEEE Trans. Robot. Automat.*, vol. 10, no. 5, pp. 670–683, Oct. 1994.
[3] B. Vanderborght et al., "Variable impedance actuators: A review," *Robot. Auton. Syst.*, vol. 61, no. 12, pp. 1601–1614, 2013.
[4] I. Aouaj, V. Padois, and A. Saccon, "Predicting the post-impact velocity of a robotic arm via rigid multibody models: An experimental study," in *Proc. IEEE Int. Conf. Robot. Automat.*, Xi'an, China, 2021, pp. 2264–2271.
[5] C. A. Rey Arias, W. Weekers, M. Morganti, V. Padois, and A. Saccon, "Refined post-impact velocity prediction for torque-controlled flexible-joint robots," submitted to IEEE Robot. Automat. Lett., 2023. [Online]. Available: https://hal.science/hal-04148817
[6] Y. Wang, N. Dehio, and A. Kheddar, "On inverse inertia matrix and contact-force model for robotic manipulators at normal impacts," *IEEE Robot. Autom. Lett.*, vol. 7, no. 2, pp. 3648–3655, Apr. 2022.
[7] Y. Wang, N. Dehio, and A. Kheddar, "Predicting impact-induced joint velocity jumps on kinematic-controlled manipulator," *IEEE Robot. Autom. Lett.*, vol. 7, no. 3, pp. 6226–6233, Jul. 2022.
[8] B. Proper, A. Kurdas, S. Abdolshah, S. Haddadin, and A. Saccon, "Aim-aware collision monitoring: Discriminating between expected and unexpected post-impact behaviors," *IEEE Robot. Automat. Lett.*, vol. 8, no. 8, pp. 4609–4616, Aug. 2023.
[9] J.-P. Sleiman, J. Carius, R. Grandia, M. Wermelinger, and M. Hutter, "Contact-implicit trajectory optimization for dynamic object manipulation," in *Proc. IEEE/RSJ Int. Conf. On Intell. Robots and Syst.*, 2019, pp. 6814–6821.
[10] T. Stouraitis, L. Yan, J. Moura, M. Gienger, and S. Vijayakumar, "Multi-mode trajectory optimization for impact-aware manipulation," in *Proc. IEEE/RSJ Int. Conf. Intell. Robots and Syst.*, 2020, pp. 9425–9432.
[11] W. Yang and M. Posa, "Impact invariant control with applications to bipedal locomotion," in *Proc. IEEE/RSJ Int. Conf. Intell. Robots Syst.*, 2021, pp. 5151–5158.
[12] J. J. van Steen, N. van de Wouw, and A. Saccon, "Robot control for simultaneous impact tasks through time-invariant reference spreading," in *Proc. Amer. Control Conf.*, 2023, pp. 46–53.
[13] Y. Wang and M. T. Mason, "Two-dimensional rigid-body collisions with friction," *J. Appl. Mechanics*, vol. 59, no. 3, pp. 635–642, 1992.
[14] V. Bhatt and J. Koechling, "Three-dimensional frictional rigid-body impact," *J. Appl. Mechanics*, vol. 62, no. 4, pp. 893–898, 1995.
[15] Y.-B. Jia and F. Wang, "Analysis and computation of two body impact in three dimensions," *J. Comput. Nonlinear Dyn.*, vol. 12, no. 4, 2017, Art. no. 041012.
[16] B. Brogliato, *Nonsmooth Mechanics*, 2nd ed. London, U.K.: Springer, 1999.
[17] FrankaEmika, "Robot and interface specifications," Accessed: Jan. 31, 2024. [Online]. Available:https://frankaemika.github.io/docs/control_parameters.html
[18] C. Gaz, M. Cognetti, A. Oliva, P. R. Giordano, and A. D. Luca, "Dynamic identification of the Franka Emika panda robot with retrieval of feasible parameters using penalty-based optimization," *IEEE Robot. Automat. Lett.*, vol. 4, no. 4, pp. 4147–4154, Oct. 2019.